A new system for in-room image guidance in particle therapy at CNAO

Gabriele Belotti [a],[*], Matteo Rossi [a],[c], Andrea Pella [b], Pietro Cerveri [a],[c], Guido Baroni [a],[b]

[a] *Department of Electronics, Information and Bioengineering, CartCasLab, Politecnico di Milano, MI, Italy*
[b] *Bioengineering Unit - Centro Nazionale di Adroterapia Oncologica (CNAO), Pavia, PV, Italy*
[c] *Istituto Auxologico Italiano, IRCCS, Milan, Italy*

ARTICLE INFO

ABSTRACT

This paper describes the design, installation, and commissioning of an in-room imaging device developed at the Centro Nazionale di Adroterapia Oncologica (CNAO, Pavia, Italy). The system is an upgraded version of the one previously installed in 2014, and its design accounted for the experience gained in a decade of clinical practice of patient setup verification and correction through robotic-supported, off-isocenter in-room image guidance. The system's basic feature consists of image-based setup correction through 2D/3D and 3D/3D registration through a dedicated HW/SW platform. The major update with respect to the device already under clinical usage resides in the implementation of a functionality for extending the field of view of the reconstructed Cone Beam CT (CBCT) volume, along with improved overall safety and functional optimization. We report here details on the procedures implemented for system calibration under all imaging modalities and the results of the technical and preclinical commissioning of the device performed on two different phantoms. In the technical commissioning, specific attention was given to the assessment of the accuracy with which the six-degrees-of-freedom correction vector computed at the off-isocenter imaging position was propagated to the planned isocentric irradiation geometry. During the preclinical commissioning, the entire clinical-like procedure for detecting and correcting imposed, known setup deviation was tested on an anthropomorphic radioequivalent phantom. Results showed system performance within the sub-millimeter and sub-degree range according to project specifications under each imaging modality, making it ready for clinical application.

1. Introduction

Clinicians can successfully exploit highly conformal dose delivery in external beam radiotherapy only in combination with high-accuracy in-room imaging (image guided radiation therapy, IGRT). In the case of radiation therapy with particle beams, image guidance is even more critical due to the inverse profile in dose deposition and the higher sensitivity to uncertainties [1–3]. State-of-the-art facilities are usually equipped with systems devoted to minimizing errors in patient repositioning [4–6]. Stable patient immobilization and accurate patient setup are required to provide a precise target alignment to the beam line. In an IGRT approach to patient treatment, images are acquired daily to guide rigid six-degrees-of-freedom (DoF) setup corrections toward the planned patient position and orientation. The practical implementation of IGRT protocols in particle therapy must account for the lack of standardized

layouts of treatment bunkers, w.r.t. conventional photon and commercial proton therapy centers [4,7]. Considerations on the cost-effectiveness of particle therapy resulted in a variety of designs, as a function of costs, of the selected particle projector (gantry vs. fixed beams) [7], the number of treatment rooms, and patient throughput optimization (in-room vs. remote imaging) [5,8–10].

In general, there is hardly a standard solution for image guidance that can be applied at every particle therapy center. Historically, patient positioning in ion-beam therapy is achieved through stereotactic registration using isocentric lasers and optical tracking systems. Setup correction is then iteratively conducted upon orthogonal kV X-ray projections or using in-room CT or cone-beam CT (CBCT) scanners [7].

The lack of a dominant standard also applies to modern non-commercial proton and ion therapy centers. For instance, the National Institute of Radiological Sciences features an in-room CT [11], while the

---

* Corresponding author.
E-mail address: gabriele.belotti@polimi.it (G. Belotti).
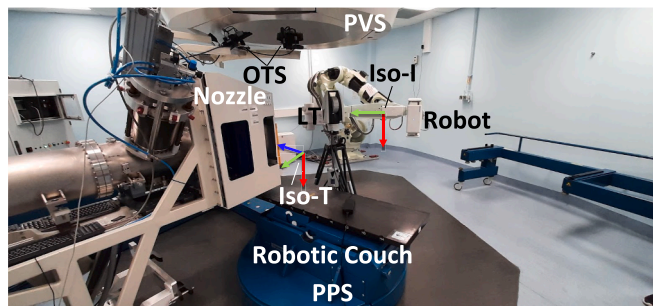
Fig. 1. CNAO treatment room 1. Imaging isocenter (Iso-I) being localized w.r.t. the treatment one (Iso-T) using a laser tracker (LT). Horizontal line nozzle and ceiling-mounted 2D/3D Patient Verification System (PVS) X-ray imaging solution by Schäer is visible as well.

treatment rooms at HIT (Heidelberg Ion Therapy Center, Heidelberg, DE) have different layouts developed explicitly for both gantry and fixed beam lines [12,13]. Conversely, MedAustron recently employed the PAIR couch-mounted CBCT system [14], and a custom robotic solution for double kV projections and CBCT off-isocenter imaging was deployed at Centro Nazionale di Adroterapia Oncologica (CNAO) [15].

The system at CNAO has been operating since 2013 in the central room (Room #2), equipped with one horizontal and one vertical fixed beam lines [16,17], thus supporting more complex treatment geometries with respect to the other two rooms featuring one single horizontal fixed beam line [18]. As a consequence, functional specifications of the in-room imaging system in CNAO Room #2 included not only patient setup verification based on two planar kV projections and 2D/3D image registration (as in the other two rooms) but also CBCT imaging and full volumetric image registration [15]. Current clinical workflow in CNAO Room #2 limits CBCT scans at the clinician's discretion, mainly to trigger off-line plan re-evaluation. This is mainly due to a major limitation of the device, which does not feature a Field-of-View (FOV) extension strategy for the CBCT. Due to geometrical constraints linked to the reduced space available in the treatment room, only CBCT with a symmetrical beam centered along the source-to-detector axis can be acquired. This commonly defined Full-Fan (FF) strategy often suffers from truncation [19] and missing information in the axial plane of the reconstructed image, especially when extracranial anatomical districts are imaged. Such limited FOV is critical in Particle Therapy because it prevents the imaging of the complete particle beam path.

Despite this limitation, the possibility to assess qualitatively and quantitatively the discrepancies in patient anatomy at the time of treatment with respect to the planning CT (pCT) including soft tissues turned out to be so relevant in terms of treatment geometry quality

verification that a new custom robotic CBCT system to be installed in one of the lateral rooms (CNAO Room #1) was commissioned. Main functional requirements of the new system were the overall capability of patient setup recovery within clinical specifications (1 mm in translation, 1° in rotations), the FOV enlargement on the axial plane, and an improved anticollision system for higher safety. In addition, the system had to be designed to co-exist and be integrated with the already installed devices in the treatment room (patient positioning system – PPS – [6], infrared optical tracking system – OTS [20,21] – and the current 2D/3D image-based patient verification system, PVS [6]) and the installation and commissioning had to be performed without interrupting the clinical activity of the selected treatment room.

The larger CBCT FOV requirement was achieved by implementing a FOV extension strategy based on a displaced detector called Half-Fan (HF) [22,23], which was based on a previously simulated [24] double complementary scan using a less-than 360° range for each acquisition, later also described by Karius et al. [25]. The safety upgrade allowed us to achieve faster robotic motion while mitigating the risk of harm from possible collisions.

This paper reports the design, calibration, and commissioning procedures performed for this custom in-room imaging system with volumetric capabilities applied to radiation treatments with accelerated particles. Moreover, we provide details concerning system key components and the obtained gain in the CBCT FOV, along with the results of measurement campaigns and commissioning activities aimed at (i) assessing the geometrical accuracy of the system and (ii) verifying accurate setup correction in clinical-like conditions under repeated setup error simulations under all available imaging modalities.

2. Materials and methods

2.1. Design of the system

The CNAO treatment Room #1 layout provides limited operating space near the beamline, as shown in Fig. 1. Therefore, the in-room imaging device installation was defined such that images could be acquired approximately two meters away from the treatment isocenter (*Iso-T*), whose definition and QA have been previously described [6,26]. As for Room #2, a remote imaging isocenter (*Iso-I*) was defined in the treatment room reference frame relying on laser tracker measurements with 0.01 mm/m accuracy (LTD 960, Leica Geosystems, Zürich, Switzerland) according to the procedures already described in [6,15,26]. The workflow envisages that after initial isocentric setup assisted by laser line alignment on references marked on the immobilization mask at a predefined configuration, typically coinciding with one of the irradiation fields, the pantographic patient positioning system (PPS) transports the patient to the Iso-I location for image-based setup
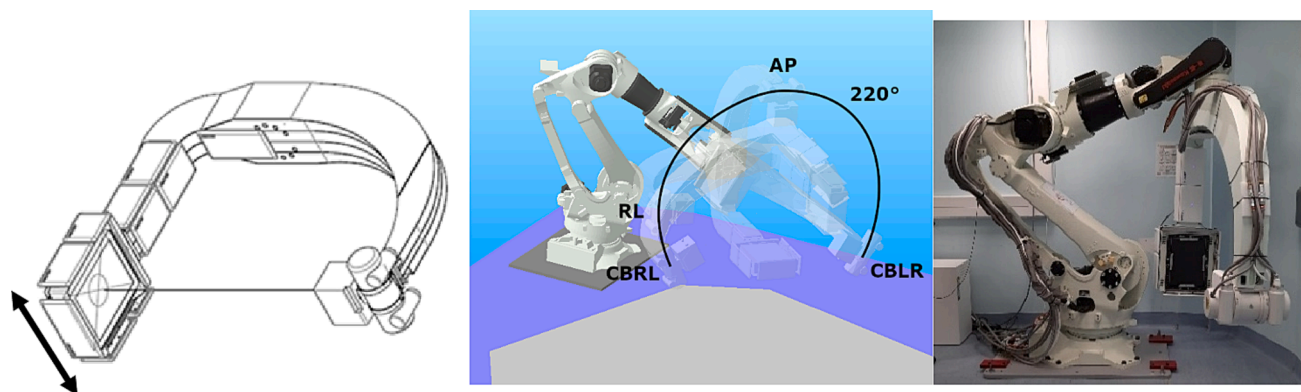
Fig. 2. (left panel) CAD of the designed C-arm where tube, collimator, and FPD are depicted. Note the black arrow highlighting the displacement directions for the FPD; (central panel) rendering with robot pose definitions and source trajectory visualization. The nomenclature follows the source to panel convention (e.g. Right to Left RL or Cone Beam Left to Right CBLR); (right panel) robot in parked layout after installation and chemical anchoring.

Fig. 3. (left panel) Robot motion pendant with emergency button and key activation switch turned to the off position. (central panel) Generator control board with static exposure button. (right panel) Continuous emission pedal used by the operator during CBCT acquisitions.

correction. Commissioning details for the PPS have been extensively presented, demonstrating how sub-millimeter residual errors are granted and assessed during daily clinical QA operations [6,20].

The imaging system consists of an articulated serial manipulator with seven joints, mounting a custom-designed C-arm structure with a kV X-ray tube, dynamic collimator, and a displaceable flat panel with pulsed fluoroscopy capabilities (Fig. 2, left panel). The installed robot was a BX300L by Kawasaki, which offers a payload of 300 kg, high accuracy in repeatability (0.3 mm at maximum speed and load), and a peak linear velocity of 2500 mm/s.

The custom C-arm was commissioned and manufactured by a third-party company. The layout is depicted in Fig. 2, left panel. The structure was designed as a trussed structured C-arm made of S235 JR (UNI EN 10027–1) steel ($E = 2.05*10^6 N/mm^2$; $\nu = 0.3$; $G = 80*10^3 N/mm^2$) to maximize the rigidity/weight ratio of the construction. Such a material reports a breaking load of $360 \div 510 \, N/mm^2$. The geometry layout was optimized for clinical image acquisition using a prototype version of the arc: the tube-isocenter distance (Source-to-Isocenter Distance, SID) was fixed at 1100 mm, whereas the Isocenter-to-Detector Distance (IDD) was 500 mm. This resulted in an overall 1600 mm Source-to-Detector Distance (SDD). The C-shape depth was defined to be 1240 mm. A metal housing for a Flat Panel Detector (FPD) was equipped with a railing system allowing lateral displacements (see Fig. 2, left panel) via a gearbox connected to a stepper motor controlled by the seventh joint of the robot. Momentum and inertia were quantified before manufacturing by simulating realistic loads of 182.8 kg. The structure was supposed to be posteriorly connected with the robot during simulations.

The C-arm holds the X-ray assembly (tube-housing-dynamic collimator) at the extremity of a branch and the FPD on the opposite side. In detail, the mounted X-ray tube was an A292 with B130H housing (Varian Medical Systems, Palo Alto, CA, USA); its total weight, also considering the mounting trunnion ring, is approximately 30 kg. This model was chosen over the A277 of the previous system by considering the maximum anode angle guaranteed by the manufacturer ($12°$ vs. $7°$), sufficient for Half Fan (HF) acquisitions. A dynamic collimator (R 221 ACS with R 225 housing, Ralco, Biassono [MI], Italy) was fitted on the tube housing to chase the FPD position. The system was fitted with a Varian 4030D FPD, with a sensible surface of 40x30 cm (Superior-Inferior $\times$ LateroLateral).

The entire system was supplied with an High Frequency series generator (SEDECAL, Algete [MD], Spain) providing up to 150 kVp, 800 mA, 80 kW, and a heat exchanger (Varian HE-101) installed inside the treatment room, close to the robot. This choice was made considering the maximum possible distance (approximately 10 m) between the X-ray tube and heat exchanger to work properly in continuous mode. The

resulting layout after installation with chemical anchoring is depicted in Fig. 2, right panel.

Fattori et al. [15] developed an in-house software suite for image-based patient alignment, that was upgraded to assist the patient setup in the clinical routine. Robot motions are requested from the software's Graphical User Interface (GUI) and activated through a pendant (left panel, Fig. 3). The X-ray emission is mastered through a separate control board with a button for static and a pedal for continuous acquisitions (Fig. 3).

2.2. In-room imaging workflow

Geometrical constraints, similar to those reported by Fattori et al. [15] were faced also in Room #1 due to the simultaneous presence of the nozzle of the horizontal beamline and the cylindrical structure of the pre-existing X-ray system for setup verification [20]. The off-isocenter imaging strategy, described in the previous paragraph (3.1) and depicted in Fig. 1, granted sufficient room for multiple 2D projections acquisition and 3D short scan (~220°) imaging capability, exploiting the rotation of the C-arm.

Daily QA and patient setup procedures for the new system follow the standard CNAO practice and are thoroughly described in previous works [6,15,26]. Hereafter, we recall the basic steps of the clinical workflow, which also replicate what is implemented and in clinical use for the device in Room #2, with a focus on the specific functionalities implemented for the new system in Room #1.

1. The treatment couch carrying the patient fitted in the immobilization mask and brought into the treatment room by means of a dedicated transport system is docked to the patient positioning system (PPS) [6].
2. The PPS is driven to the initial isocentric setup configuration retrieved from the treatment plan for qualitative verification of isocentric laser lines alignment on marked reference on the immobilization mask and eventual preliminary setup verification by means of the Optical Tracking System (OTS).
3. PPS is driven into a "*safe*" configuration outside the working volume of the robotic imaging device.
4. The imaging robotic device is driven from its Parking Position to the Antero Posterior (AP) configuration, ready for acquiring the first kV projection.
5. The robotic couch is driven to the imaging configuration at Iso-I. This configuration is automatically calculated accounting for the patient-specific isocentric setup configuration (different for every patient), the measured relative position of Iso-T with respect to

Iso-I, and the direction of the rotation axis of the C-arm in the room isocentric space (see paragraph 3.1 Design *of the system*' and Fattori et al. [15]).

6. **Static image-based setup verification** (kV projections and 2D/3D registration):
   a. AP projection is acquired.
   b. The robotic device is driven to the Latero-lateral (LR) configuration by a single joint 90° rotation of the C-arm.
   c. LR projection is acquired.
   d. 2D/3D image registration is launched through the GUI of the SW application after initial manual alignment.
   e. The obtained 6 DoF correction vector is automatically propagated to all the irradiation field PPS configurations retrieved from the treatment plan [15].
   f. AP and LR projections acquisition and 2D/3D registration may be repeated until the calculated correction vector components fall below clinically relevant thresholds (0.3 mm and 0.3°).

7. Alternatively, or following the static setup verification (step 6), **Dynamic image-based setup verification** (CBCT and 3D/3D registration):
   a. FF modality:
      i. With PPS in the imaging configuration (Iso-I), the C-arm is brought to the initial dynamic rotation pose (named CBRL and shown in Fig. 2).
      ii. The FF CBCT scan is performed by rotating the C-arm about the sixth joint of the robot for 220° while the operator presses the X-ray emission control pedal, stopping in the final dynamic pose (CBLR, shown in Fig. 2). While the C-arm is rotated back to the RL pose, the dedicated algorithm finishes the reconstruction of the CBCT volume.
      iii. 3D/3D image registration is launched in the GUI of the SW application after initial manual alignment.
      iv. The obtained 6 DoF correction vector is automatically propagated to all the irradiation field PPS configurations retrieved from the treatment plan [15].
      v. FF acquisition and 3D/3D registration may be repeated until the calculated correction vector components fall below clinically relevant thresholds (0.3 mm and 0.3°).
   b. HF modality:
    i. With PPS in the imaging configuration (Iso-I), the C-arm is brought to the CBRL pose.
    ii. The FPD is offset laterally by the dedicated stepper motor in the right direction (+120 mm).
    iii. The first HF CBCT scan is performed by rotating the C-arm clockwise about the sixth joint of the robot for 220° during continuous exposure stopping in the CBLR pose. While the panel moves left bound (from + 120 mm to −120 mm), the dedicated algorithm finishes reconstructing the first part of the CBCT volume.
    iv. The second HF CBCT scan is performed by rotating the C-arm counterclockwise about the sixth joint of the robot for 220° during continuous exposure stopping in the CBRL pose. While the panel aligns back to the FF configuration and the C-arm resets to the RL pose, the dedicated algorithm finishes reconstructing the second part of the CBCT volume.
    v. 3D/3D image registration is launched in the GUI of the SW application after initial manual alignment.
    vi. The obtained 6 DoF correction vector is automatically propagated to all the irradiation field PPS configurations retrieved from the treatment plan [15].
    vii. HF acquisition and 3D/3D registration may be repeated until the calculated correction vector components fall below clinically relevant thresholds (0.3 mm and 0.3°).

8. PPS is driven to the "safe" position.
9. The robotic imaging device is driven to the Parking Position.

10. PPS is driven to the corrected treatment configuration.

The entire workflow, in terms of both PPS and robotic imaging device motion, was designed to minimize the risk of undesired collisions by separating the PPS and the robotic device motion as much as possible. In any case, several safety redundant controls were integrated into the system, later described in section '*3.3 Safety aspects*'.

2.2.1. Images

The FPD and the X-ray source are synchronized through a hardware connection, ensuring a repeatable exposure. Exposure parameters, such as time (ms), tube voltage (kV), and tube current (mA), can be adjusted in the GUI, and thanks to the experience from the Room #2 system, several presets are available depending on the robot pose and anatomical district. Planar radiographies are acquired at full resolution (pixel spacing $\Delta u = \Delta v = 0.194$ mm, 2048x1536 pixels, 273x205 mm at isocenter) at AP and RL positions at user request by pressing the dedicated button on the X-ray emission board. The in-house software integrates the 2D/3D registration algorithm developed by Steininger et al. [27] and is made available through the Plastimatch open-source project [28]. This software produces Digitally Reconstructed Radiographies (DRRs) from the CT used for treatment planning by means of a forward projection implementation on a Graphical Processing Unit (GPU). The DRRs drawn at AP and RL geometries are then registered rigidly to the actual radiographies by minimizing the gradient difference between the two images. The registration is manually initialized, and considering also the automatic registration runtime, the total elapsed time stays under 1 min.

For the CBCT in both modalities (FF and HF), the continuous acquisition produces a set of projections at halved resolution (pixel spacing: $\Delta u = \Delta v = 0.388$ mm, size: 1024x768, 273x205 mm at isocenter). IN FF mode, around 450 projections are acquired during the 220° rotation of the sixth joint of the robot as the operator presses on the dedicated pedal for continuous X-ray emission. A single continuous acquisition is performed in 30 s, with the C-arm rotating at 7.3°/sec with the FPD set to a 15 Hz framerate. Hence, projections are sampled at 0.49° intervals.

Volumetric image reconstruction is performed using a GPU implementation of the Feldkamp-Davis-Kress (FDK) [29] based on the RTK open-source software [30]. The dedicated workstation mounts 16 GB of RAM, an Intel Xeon W-2133 CPU (3.6 GHz clock), and an Nvidia 1080 GPU with 8 GB of dedicated VRAM. The final CBCT image is reconstructed before the C-arm returns to the RL position (steps 7.a.ii or 7.b.iv in 3.2 In-room *imaging workflow*'). The image is automatically masked to the Field-of-View pseudo cylinder size (SuperioInferior-SI: 271 mm, axial diameter in FF/AP-RL: 204 mm, axial diameter in HF/AP-RL: 403 mm). The masked CBCT image is then overlayed onto the pCT previously loaded and displayed in the SW GUI from the DICOM files. Loaded CBCT images can be manually aligned and then automatically superimposed via a 3D/3D multi-resolution voxel-based rigid registration. The algorithm consists of three stages of minimization of Normalized Mutual Information using an Amoeba optimizer with isotropic sub-sampling grids from 3 mm to 1 mm. The time required for registration (manual initialization plus automatic registration) depends upon the operator but is typically performed within 1 min.

2.2.2. CBCT resolution choice

Since the spatial resolution of the reconstructed CBCT volume influences the computational time required for the reconstruction, a trade-off between the two specifications had to be found. The choice also took into consideration the typical spatial resolution of the planning CT (up to 0.98x0.98x1 mm) and a clinically acceptable computational time. A Catphan 504 phantom (CatPhan; The Phantom Laboratory, Salem, NY, USA) was imaged in the two CBCT modalities to assess reconstruction time as a function of effective image resolution. The High-Resolution module CTP528 was used to visually evaluate line pairs at various pixel spacing and subsequently set the standard solution for the system's

Fig. 4. Detail of the anticollision system mounted on the flat panel chassis.

CBCT scans. Results are presented in section '4.1 CBCT resolution choice trade-off'.

2.3. Safety aspects

Safety aspects gain the highest importance when industrial-derived robotic devices are used in a clinical environment. The primary concern is represented by robot motion close to operators and patients. In this respect, the described installation inherited safety measures already implemented for the system operating in Room #2. Namely, an additional module (Kawasaki Cubic-S) is installed in the robot controller. This module complies with ISO10218-1, 13849-1 (PLd/ Category 3), and IEC61508 (SIL2) and is responsible for ensuring safety by monitoring and stopping the robot's motion in the event of unauthorized movement or unexpected conditions. It allows defining and real-time monitoring of allowed and prohibited areas within the robot workspace, thus minimizing the risk of unexpected collision between the system and other instrumentation in case of control primary motion control failures. We used this safety component also to inhibit the contemporary motion of the robot and the PPS.

The C-arm side mounting the flat panel detector was equipped with an anticollision system composed of AIRSKIN modules (Blue Danube Robotics GmbH, Wien, Austria). This location is considered the most critical as it is the closest to the subject under treatment (see Fig. 4). The AIRSKIN modules consist of soft pads that continuously monitor the pressure through a dedicated control unit and trigger an emergency stop within 9 ms whenever a force over 5 N is registered. These pads are compliant with EN/ISO 13849–1 (PL e / Cat. 3) and EN/IEC 62,061 (SIL 3). At top speed during CBCT acquisition, this results in a $0.066°$ delay in response. Thanks to this, the robot stops after a maximum linear travel of 0.6 mm and 1.3 mm at the panel and tube level, respectively.

Possible emergencies stemming from unexpected collisions or Cubic-S intervention can be recovered from the treatment room or the local control room. Independent pendants are present there with key selection for single pendant activation.

Additional controls were added regarding X-ray hazards to ensure the operator and patient safety. When the operator requests a static or continuous acquisition, the collimator automatically reaches the predefined configuration according to the flat panel position (as is the case for CBCT in HF modality) through CANBus communication. As for all the X-ray equipment operating in CNAO treatment rooms as well as for the therapeutic beam production, the device is interfaced with the CNAO interlock system that inhibits exposure in case all the safety conditions are not verified (e.g., the treatment room door is open, personnel is inside the treatment room).

2.4. X-ray calibration procedures

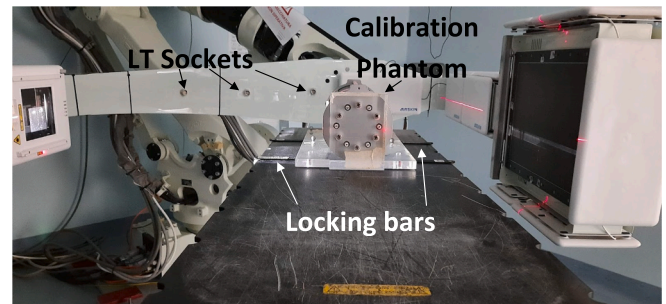The camera pose describing the imaging geometry was determined

Fig. 5. Geometric X-ray phantom setup for calibration procedures at Iso-I. Note the locking bars that link the phantom base to the carbon-fiber couch top and ensure a repeatable pose. Additionally, three laser tracker sockets are visible on the left side of the C-arm.

through a process of calibration of the projective parameters, which was implemented following the well know Flexmap approach [31,32], extended to 9-DoF w.r.t. the system operating in Room #2 for higher accuracy [15]. This calibration method requires prior knowledge of a cloud of points embedded in a calibration phantom. Given an image of the object, the algorithm requires an initial guess for each parameter, which is derived from the C-arm nominal geometry. The geometrical parameters are used to forward-project the known cloud of points onto the image plane. After an automatic point detection on the acquired image, the parameters are iterated with a Levenberg-Marquardt optimizer. The merit function which is minimized is the cartesian distance (as RMSE) between detected points and forward-projected fiducials. Our approach relies on a geometric X-ray phantom (Model 2008; Brandis Medizintechnik Vertriebs GmbH, Weinheim, Germany) with 37 embedded ball bearings (BBs, Fig. 5)[6].

The calibration procedure envisages the positioning of the phantom on the treatment couch, which, jointly with the PPS, is driven in a predefined configuration that grants that the central bead embedded in the phantom coincides with the treatment room isocenter. This alignment is ensured by laser tracking measurements of phantom external features solidly linked to the embedded beads configuration [6,26]. The PPS is then driven to the Iso-I position, according to predefined parameters of the PPS configuration, ensuring that the central beed embedded in the phantom coincides with the center of rotation of the C-arm. Again, this requirement is obtained by repeated laser tracker measurements during multiple C-arm rotations and poses (see the available laser tracker measuring points in Fig. 5). Gravity-induced deviations during motion are minimized by the C-arm design and material choices and, in any case, considered repeatable due to the constant payload at the C-arm extremities, thus included in the calibration parameters estimation.

For static imaging (AP, RL, or LR projections), calibration was
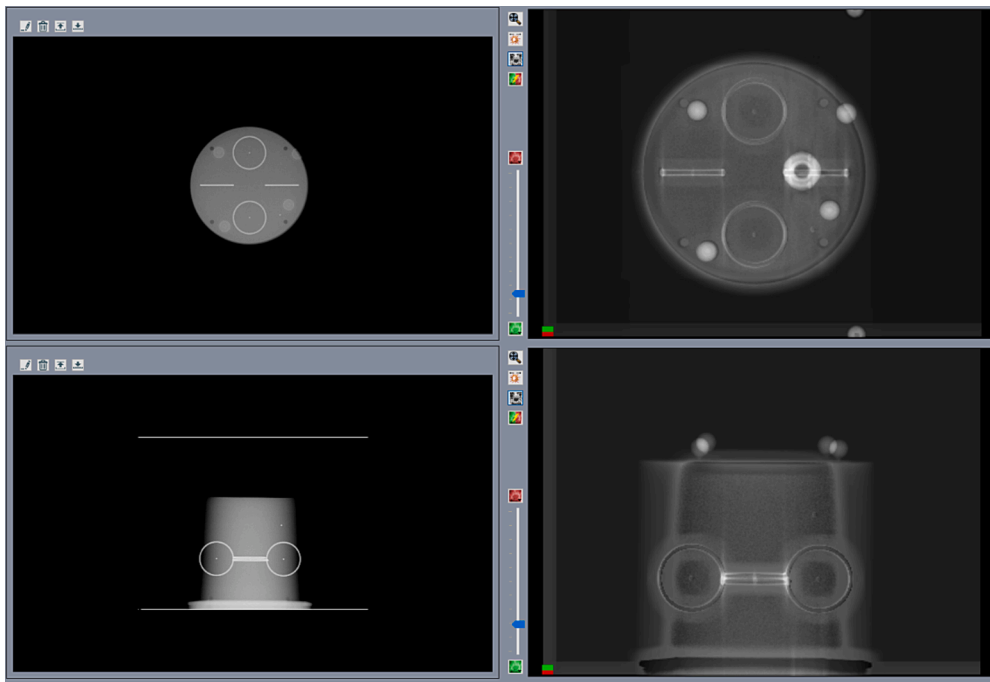
Fig. 6. Aligment of RING phantom using the in-house software based on the Reg2-3 platform. On the left, AP (up) and RL (down) acquired projections are displayed. In the corresponding panels on the right the DRRs are superimposed to the planar X-rays. Radiopaque IR markers can also be identified in the DRRs.

carried out for each acquired image as follows:

1. Image acquisition with predefined exposure settings (85 kVp, 100 mA, 8 ms).
2. Overlay of nominal BBs coordinates, according to the nominal angle of the robot wrist ($\pm 90°$ for RL/LR and $0°$ for the AP configurations, respectively).
3. Manual drag-and-drop of projected BBs to match the acquired image to initialize the procedure.
4. Extraction of BBs centroids from the acquired image, relying on a local window centered in the projected points.
5. Iterative optimization of calibration parameters to minimize the back-projection errors (projected vs. extracted BBs coordinates).

A similar procedure was implemented to calibrate the imaging system for CBCT acquisition. In this case, image acquisition is carried out continuously over a rotational range of $220°$. Manual initialization (drag-and-drop) is performed only for the first acquired image, relying on the final calibration parameters of the previous projection for
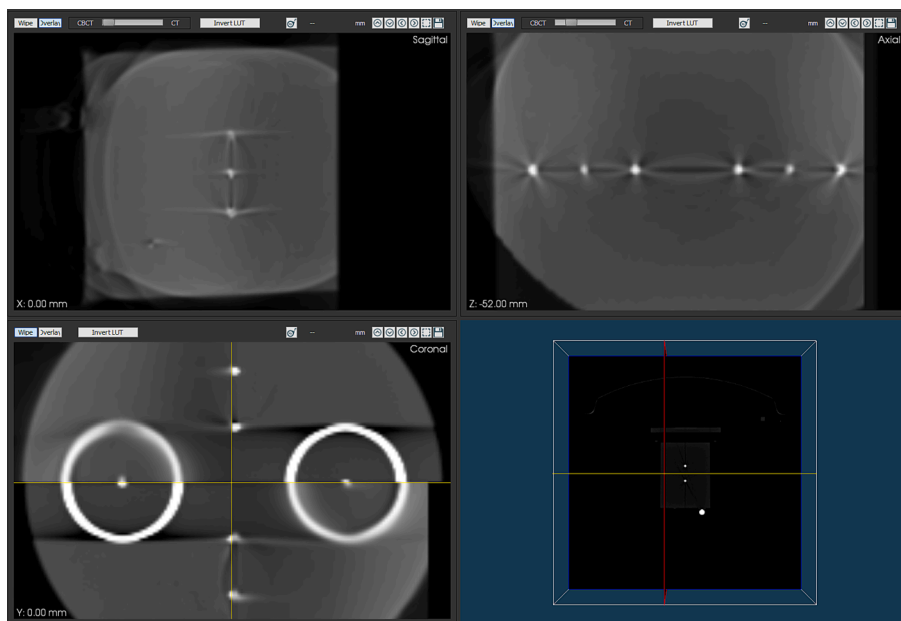
Fig. 7. Aligment of RING phantom using the in-house software in the CBCT modality. Sagittal (up, left), Axial (up, right) and Coronal (bottom, left) views are rendered, displaying the RING phantom in the pCT overlayed on the acquired in-room CBCT. A 3D render of the pCT is visible in the interaction window (bottom, right).

initializing the ones of the following projection. Per-projection parameters are smoothed to reduce optimization drifts with a moving average window of 10 projections. Separate calibrations were performed for the FF modality and for each of the rotational motions required for HF CBCT. The calibration algorithm is available at https://github.com/mrossi93/geometric_calibration. Similarly to the system operating in Room #2, the issue of the lack of repeatability of gantry angles across multiple rotational acquisitions was overcome by linear interpolation to estimate the projective parameters at predefined C-arm angles [15].

The system is regularly calibrated during periodic maintenance shifts scheduled two times per year. Daily QAs are performed on the calibration phantom, assessing alignment residuals at Iso-I. The unscheduled recalibration of any of the imaging modalities is triggered by discrepancies above 0.5 mm / 0.5°.

2.5. Technical commissioning of the system

The technical commissioning of the system was mainly focused on the accuracy assessment of the mapping parameters between the Iso-I and Iso-T reference systems, estimated through the above-mentioned laser tracker measurements, and the consistency of setup correction parameters across imaging and image registration modalities.

Technical commissioning tests were designed on the positioning phantom P43029 (PTW-Freiburg, Germany), consisting of a PMMA cylinder phantom featuring four inner reference steel rings and a set of four spherical OTS-compatible IR and radiopaque markers. The phantom (which will be referred to as RING phantom from now on) was imaged with the CNAO CT system (Siemens Somaton, from Siemens Healthcare GmbH., Erlangen, Germany) with 0.98x0.98x1 mm spatial resolution. pCT series were then used to define a purely geometric treatment plan by means of the treatment planning software available at CNAO (Raystation, from RaySearch Laboratories AB, Stockholm, Sweden), which allowed defining the PPS configuration bringing the center of one of the steel rings center to coincide with the treatment room isocenter (Iso-T), representing the treatment nominal condition. Setup errors for the assessment of the consistency between different imaging modalities were simulated by adding known translational and rotational shifts to the PPS nominal configuration.

2.5.1. Consistency of imaging and treatment isocenters in nominal condition

The first test set was designed in order to assess the mapping accuracy among imaging and treatment reference systems. The primary aim was to verify that image-based position correction performed at Iso-I would lead to a correct phantom positioning at Iso-T. The procedure envisaged a preliminary manual phantom alignment at Iso-T, using the laser isocentric reference lines, followed by a setup refinement at Iso-I through orthogonal X-ray acquisitions and 2D-3D registration (see Fig. 6) and a further CBCT acquisition (FF and HF) and 3D-3D registration (see Fig. 7). Results were expressed as the values of the additional correction vector parameters produced by 3D-3D registration following the 2D-3D procedure at Iso-I (expected negligible) and those detected by the optical tracking system on the external IR marker after having driven the PPS back to Iso-T. In this latter case, the residual discrepancies detected by the OTS at Iso-T allowed assessing the congruency of imaging and treatment isocenters and reference frames as well as the accuracy of the propagation of correction vectors calculated and applied at Iso-I. In order to interpret the results, it is worth recalling that the OTS system features an intrinsic accuracy in markers 3D localization around 0.3 mm [6,20,21].

2.5.2. Consistency across imaging modalities in clinical-like conditions

In this case, a set of positioning errors of the RING phantom was imposed and recovered by means of clinical-like image-based procedure. The protocol envisaged phantom positioning at Iso-T with the aid of isocentric laser lines alignment and OTS optical guidance. Then, a set of

Table 1
Disk usage and average computational time for the FDK algorithm depending on the chosen resolution of the final volume. Reconstruction time is reported for a single scan, i.e., in the case of a single complementary HF or a FF reconstruction.

Axial resolution [mm]	Reconstruction time [s]	Size (FF/HF) [MB]	Line Pairs [lp/cm]
1.0x1.0	20	42 / 250	4
0.9x0.9	21	51 / 309	4
0.8x0.8	22	65 / 390	4
0.7x0.7	23	85 / 510	4
0.6x0.6	26	116 / 694	5
0.5x0.5	29	166/ 1,000	5
0.4x0.4	40	260/ 1,562	5
0.3x0.3	51	462 / 2,778	5
0.2x0.2	92	1,039 / 6,250	6
0.1x0.1	309	4.159/ 25,000	6

five composite 6 DoF errors in the 10 mm and 2° range was imposed to the PPS. Afterward, the PPS was driven to the imaging position at Iso-I, ready for the image-based correction. For every set AP/RL static radiographies, CBCT FF and CBCT HF were acquired, followed by automatic registration for each imaging modality, in this specific order. Correction vectors estimated by 3D/3D registration with every parameter under the 0.3 mm/ 0.3° threshold were considered negligible and were not applied. Test results for the X-ray imaging pipeline were expressed as deviations of the correction vector from the error applied at Iso-T. Finally, after applying the correction vectors to the PPS at Iso-I, the PPS was driven back to Iso-T. This allowed to measure absolute deviations using OTS and against the original PPS configuration.

This experiment has the double purpose of verifying consistency across imaging modalities, testified by neglectable 3D/3D based refinements, and the accurate transformation to the treatment room coordinate system, thanks to the information gathered from the PPS and the OTS.

2.6. Preclinical phantom study

The technical system commissioning was followed by a more clinical-like commissioning procedure using an anthropomorphic radioequivalent phantom. The main aims were the testing of the entire image-based setup errors detection and correction pipeline, mimicking the envisaged clinical workflow under all the implemented imaging modalities. For this aim, a clinically realistic treatment plan was elaborated on the pCT series acquired on the pelvis district (slice 27 to slice 38, 0.98x0.98x1 mm resolution) of the ATOM M701 adult male radioequivalent anatomical phantom (CIRS, Norfolk, VA, USA). The phantom was also fitted with five IR markers for preliminary optical OTS alignment.

The protocol envisaged the phantom alignment at Iso-T by means of isocentric laser lines and OTS, the subsequent driving of the PPS to Iso-I, and a further setup refinement through 2D/3D automatic registration. At Iso-I, eight composed 6 DoF errors in the range 10 mm and 3° were applied and subsequently recovered under all imaging modalities. Two acquisitions per modality were performed, one for the initial correction and one for verification and possible further correction, especially for large imposed errors. Results were expressed as the deviations of the estimated correction vector parameters with respect to the imposed error. CBCT in HF modality allowed assessing the advantages of an extended FOV in the phantom pelvic district, with notably improved accuracy in image-based error recovery with respect to the CBCT FF modality, as described in section 4.3.
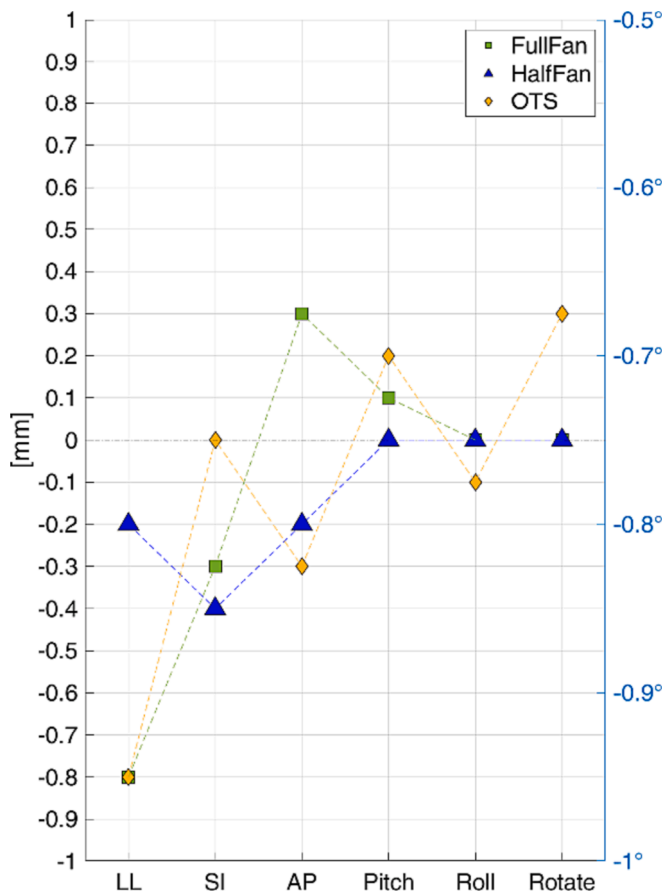
3. Results

3.1. CBCT resolution choice trade-off

According to the results reported in Table 1, the CBCT reconstruction
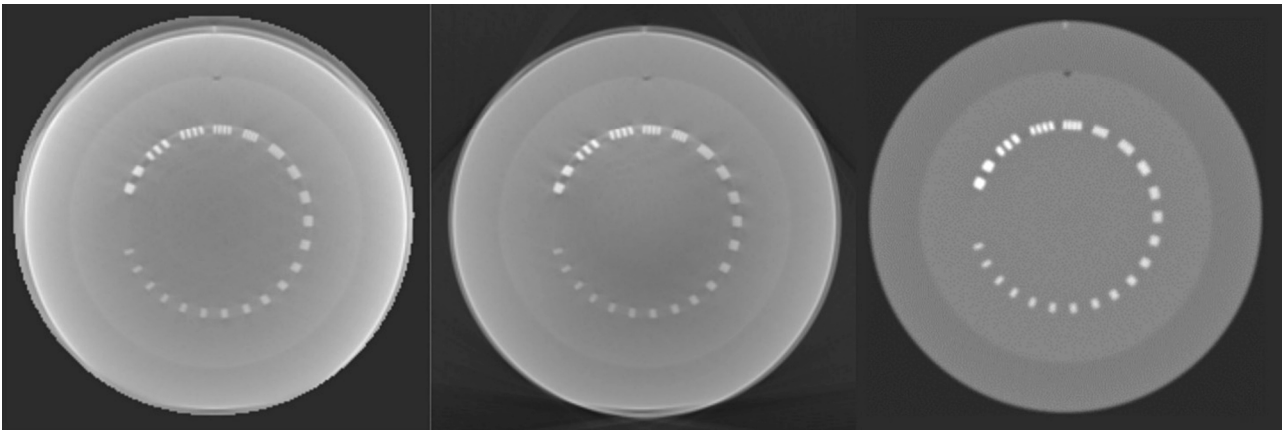
Fig. 8. Exemplary slice of Catphan High-Resolution Module 528 imaged by the scanner and reconstructed at 1x1x1 mm resolution using FF (left) and HF (center) protocols, compared against the pCT reference (right) at 0.98x0.98x1 mm resolution. Notably, border effects on the boundaries of imaged object are present. These are due to the FPD oversaturation.

Fig. 9. Setup accuracy in nominal conditions. Translation and rotation errors are reported here about the anatomical axes Latero-Lateral (LL/pitch), Superior-Inferior (SI/Roll), and Anterior-Posterior (AP/Rotate). Residuals were measured by the 3D/3D registration pipeline (FF/HF) and the OTS on the RING phantom aligned to nominal conditions using the 2D/3D registration pipeline.

Table 2

Mean absolute difference between imposed error and applied X-ray-based correction (first column), OTS measured residuals at Iso-T (central column) and PPS deviations from the planned setup configuration (right column).
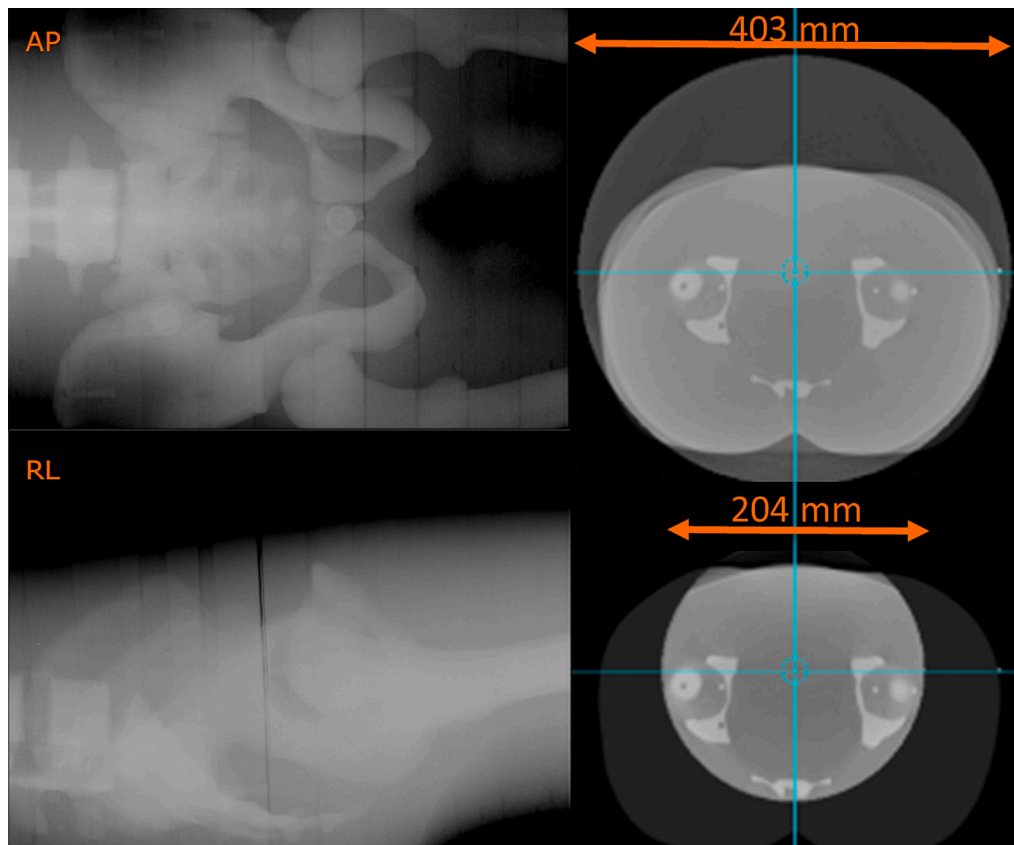
	Residual error	OTS residuals	PPS deviations
LL (mm)	0.4 ± 0.2	0.3 ± 0.3	0.3 ± 0.2
SI (mm)	0.3 ± 0.2	0.3 ± 0.2	0.2 ± 0.2
AP (mm)	0.3 ± 0.2	0.4 ± 0.3	0.2 ± 0.2
Pitch (°)	0.2 ± 0.2	0.1 ± 0.1	0.3 ± 0.3
Roll (°)	0.2 ± 0.2	0.3 ± 0.3	0.1 ± 0.1
Rotate (°)	0.1 ± 0.1	0.1 ± 0.1	0.1 ± 0.1

resolution of the CT series used for treatment planning (typically 0.98x0.98x1 mm). Results were consistent across the two CBCT acquisition modalities, and an example of reconstruction at 1x1x1 mm (4 lp/cm) resolution of the Catphan module CTP528 is shown in Fig. 8. These tests also allowed us to evaluate the presence of a boundary effect caused by FPD oversaturation when an object smaller than the CBCT FOV was imaged.

3.2. Setup correction residuals

Fig. 9 summarizes the results of the test described in section 3.5.1 *Consistency of imaging and treatment isocenters in nominal condition*. Submillimeter and sub-degree size of the additional correction vectors calculated by CBCT (FF and HF modality) and 3D-3D registration following the 2D-3D corrective procedure at Iso-I were found. To avoid confusion, sub 0.1 mm and sub 0.1° residuals were not plotted. These figures attest to the congruency within clinical specifications (discrepancies below 1 mm e 1°) of image-based modalities at Iso-I, resulting from different calibration procedures for camera pose estimation under the three imaging modalities. Inconsistencies detected by the OTS at Iso-T resulted within specifications, although slightly higher than in Fattori et al. [15]. It is hard to give a specific explanation since discrepancies could be caused by the composition of different factors. Above all, the image-based correction procedure at Iso-I works by forcing the superimposition of the internal structures of the phantom (the rings) with no involvement of the external IR markers in the optimization process; the slight residuals of the image-based corrective procedure (especially on the rotational components) could lead to appreciable mispositioning of the IR external markers as a function of their mutual geometrical relationships with respect to the targeted internal phantom features.

Table 2 reports the average absolute residuals (±standard deviation) of the test described in section 3.5.2 Consistency *across imaging modalities in clinical-like conditions*', designed to assess the quality of imposed

resolution was fixed at 1x1x1 mm with an acquisition time window of 30 s. The finer resolution achieved at 0.6x0.6x1 mm was insufficient to justify the additional computational time and disk space usage in clinical use, with potential user interface issues due to machine overloads during the reconstruction process. In addition, a finer resolution would not grant improvement in the 3D-3D registration accuracy due to the

Fig. 10. Pelvis phantom imaged during alignment tests. (left) Orthogonal projections at AP (top) and RL (bottom) positions. (right) Two scans performed in nominal conditions are displayed here overlayed to the planning CT. Note the FOV difference between FF (bottom) and HF (top). Border effects shown in Fig. 8 are again present here.

error detection by the three imaging modalities at Iso-I. The X-ray-based correction pipeline precision is attested by a low standard deviation ($<=$ 0.2 mm and $<=0.2°$) while its accuracy is within specification (<1 mm/ $1°$). Test were conducted with a first 2D-3D registration followed by CBCT refinement which showed consistency between modalities. In fact, only in error recovery cases 2 and 4, using FF and HF respectively, produced correction vectors above the 0.3 mm and 0.3° threshold and were subsequently applied. OTS-based measures and PPS deviations from the planned configuration were within their own specifications, thereby validating the integration of the new image-based setup correction in the treatment room.

3.3. Preclinical phantom residuals

When clinical-like tests on the radioequivalent phantoms were performed (protocol is described in section 3.6 Preclinical *phantom study*'), results confirmed the overall clinical applicability of the envisaged image-based registration pipeline with smooth transitions of the PPS from the Iso-T to the Iso-I configurations, adequate FOV dimensions for the CBCT HF modality (Fig. 10) and an overall accuracy within specifications (Fig. 11). All imaging modalities and related image-based registrations allowed estimating the imposed setup error with discrepancies below 1 mm and 1°. As expected, the 3D-3D imaging pipeline granted similar or lower discrepancies with respect to the 2D-3D procedure, except for a negligible (0.1°) underperformance in Rotate peak deviation for CBCT HF. The influence of the border effects visible on CBCT volumetric reconstructions needs to be limited by imposing adequate ROIs on the 3D-3D registration. Pitch recovery seems particularly underperforming for the 2D/3D procedure. However, for 7 measurements out of 8 Pitch absolute residual was below 0.4°. Therefore, the single 0.6° deviation, although within specification, could be an

outlier due to more pronounced weight-induced pitching on the carbon couch.

3.4. Safety and regulatory aspects

Inheriting the experience matured by the clinical application of the robotic imaging device operating in CNAO Room #2, a specific focus was given to safety measures to prevent undesired hazardous situations both for patients and operators. The main countermeasure already operative in Room #2, which proved to ensure no accidents over more than ten years of clinical use, resides in procedural optimizations such that multijoint robotic motion occurs only when a patient is outside the workspace of the robotic manipulator. Single joint, 1 DoF motion (Joint 6) for C-arm rotation is the only allowed motion with a patient within the patient-robot workspace. A certified safety component (Kawasaki Cubic-S) ensures immediate intervention in case undesired robot behavior is detected by low-level action on joint brakes and motor disabling. The reciprocal motion inhibition between PPS and robot ensures the serialization of the procedures with limited impact on the overall time required for patient setup verification and correction. Although highly improbable, a new, fast response anticollision system was designed to rapidly stop robot motion in case of contact of the C-arm with other components, operators, or patients.

Concerning the regulatory aspects related to the development and clinical application of the described system, the same approach applied to the already operating device in Room #2 was followed. The project was labeled as a CNAO internal R&D activity aiming at the development of a system for exclusive use within CNAO with no independent certification and no intentions to resell the system to third parties. Under this scenario, the device was thoroughly documented with the supervision of the CNAO Quality Service, including HW/SW functional specifications,
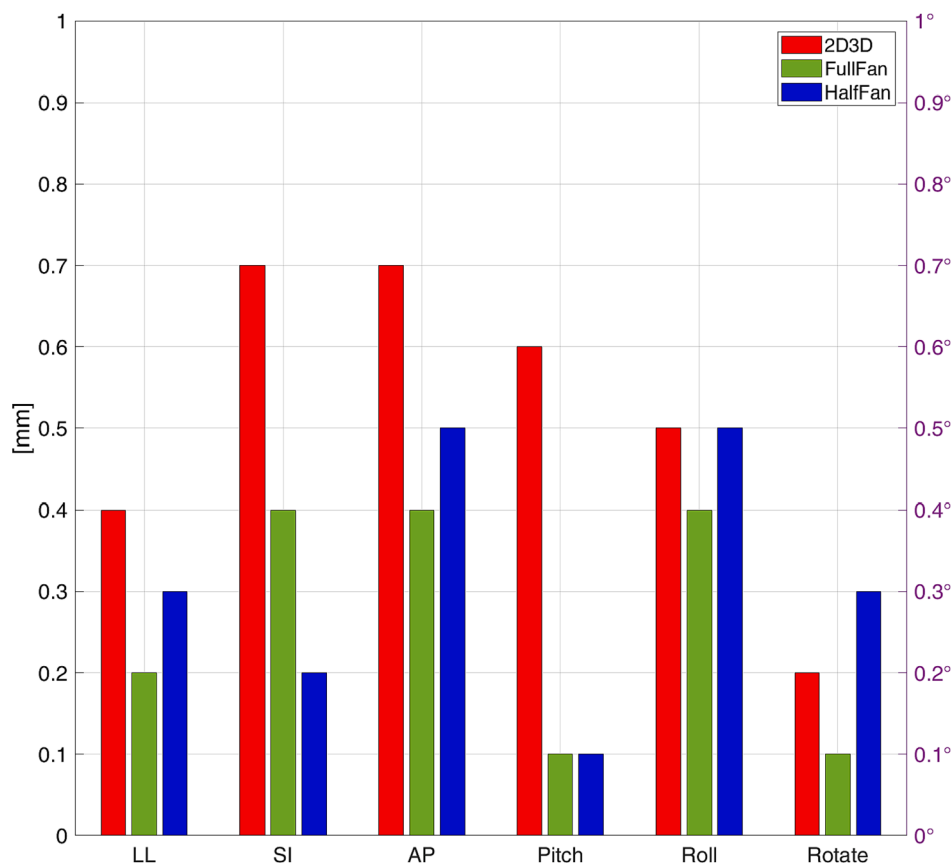
Fig. 11. Maximum absolute deviations over eight applied and recovered errors at Iso-I for each modality. Translation and rotation errors are reported here about the anatomical axes Latero-Lateral (LL/pitch), Superior-Inferior (SI/Roll), and Anterior-Posterior (AP/Rotate).

HW/SW components description, risk analysis, and countermeasures, SW testing report, and technical and preclinical commissioning reports. CNAO was responsible for verifying the implemented documents and issuing the request to the Italian Regulatory body (Istituto Superiore di Sanità, ISS) to include the device in the overall CE certification of the entire CNAO system.

4. Discussion

In this paper, we described a custom robotic C-arm for 2D and 3D in-room imaging developed, installed, and commissioned at the Centro Nazionale di Adroterapia Oncologica (CNAO) in Pavia. Results of commissioning activities and measurements carried out at CNAO facilities were reported, with a specific focus on geometric accuracy and setup error detection and correction capabilities. The system was designed for orthogonal static projection acquisitions and volumetric (CBCT) imaging with variable dimensions of the reconstructed volume. System design needed to fulfill adequate installation flexibility to operate in the fixed beamline treatment bunker with the presence of the pantographic robotic patient positioning system with a large footprint that largely limited the useful space for the in-room imaging installation. As a result, the system features in-room off-isocenter imaging and counts on the mechanical intrinsic motion accuracy of the patient positioning system (<0.3 mm and <0.3°; CE registration number V-11-048) [6] for accurate application of the estimated setup corrections at the imaging position and adequate correction propagation at irradiation positions. No treatment room downtime was required during system installation, integration, and commissioning by exploiting night shifts and routine room maintenance.

Two different commissioning protocols were performed with different phantoms. The technical commissioning was based on a

Table 3
Comparison between the two custom scanners installed at CNAO.

	Room 2 Custom Scanner [15]	New Room 1 Scanner (2023)
Acquisition protocols	2D, 3D FF	2D, 3D FF, 3D HF
2D/3D setup correction	Sub mm, sub-degree	Sub mm, sub-degree
3D/3D setup correction	Sub mm, sub-degree	Sub mm, sub-degree
Field-of-View	208 mm	204 mm / 403 mm
Continuous exposure time	40 s	30 s/30 s × 2
Reset time	20 s	15 s/5 s
Anticollision system	Bumper (22 ms delay)	Air cushions (9 ms delay)
Anode angle	7°	12°
Collimation	Static	Dynamic
Flexmap calibration	7 DoF	9 DoF

geometric phantom with embedded metal rings and aimed at verifying the system imaging geometry and related mapping parameters with respect to the isocentric treatment reference frame needed for correction propagation. All tests granted accuracy within project specifications (1 mm, 1°) under all imaging modalities. In 3D imaging, the observed boundary effects due to the oversaturation of the FPD [33] will be mitigated by a composite Al/Cu filter to be mounted at the exit window of the X-ray tube for higher image quality.

The preclinical commissioning was performed on a radioequivalent anthropomorphic phantom. Tests highlighted the clinical applicability of the entire pipeline for off-isocenter 2D and 3D imaging and related 2D/3D and 3D/3D image registration and revealed sub-millimeter and sub-degree uncertainties. With respect to the system already operating in CNAO Room #2 (Table 3), the new system grants up to two times the axial FOV with faster acquisition without loss of accuracy. CBCT FOV

enlargement was achieved by implementing Half Fan CBCT imaging modality on two 220° complementary rotations, allowing to limit the time required for projections. A higher C-arm rotation speed with respect to the system operating in Room #2 was allowed by equipping the device with a fast response anticollision system granting sufficient safety at rotational speed up to 14.6°/sec. This also allowed for decreasing the number of projections acquired for CBCT reconstruction with consequently less non-therapeutic dose delivered to the patient. The overall acquisition time for CBCT projection acquisition turned out to be similar to the one featured by commercial systems (for example, the MedPhoton ImagingRing(50 s)) [25].

5. Conclusions

The commissioned system accuracy is compatible with Particle Therapy requirements for setup correction. All imaging modalities meet the requirements and allow the planning setup geometry to be reproduced in the absence of deformations. Moreover, the additional safety, hardware, and software development allowed for the implementation of a double scan method obtaining substantial axial FOV extension in a highly customized clinical scanner while optimizing acquisition time and, thereby, reducing the non-therapeutic dose to future patients.

Declaration of Competing Interest

The authors declare that they have no known competing financial interests or personal relationships that could have appeared to influence the work reported in this paper.

Acknowledgments

References

[1] van de Water S, Kreuger R, Zenklusen S, Hug E, Lomax AJ. Tumour tracking with scanned proton beams: Assessing the accuracy and practicalities. Phys Med Biol 2009;54(21):6549–63.

[2] Engelsman M, Schwarz M, Dong L. Physics Controversies in Proton Therapy. Semin Radiat Oncol 2013;23(2):88–96.

[3] Knopf A-C, Boye D, Lomax A, Mori S. Adequate margin definition for scanned particle therapy in the incidence of intrafractional motion. Phys Med Biol 2013;58 (17):6079–94.

[4] Devicienti S, Strigari L, D'Andrea M, Benassi M, Dimiccoli V, Portaluri M. Patient positioning in the proton radiotherapy era. J Exp Clin Cancer Res 2010;29. https://doi.org/10.1186/1756-9966-29-47.

[5] Fava G, Widesott L, Fellin F, Amichetti M, Viesi V, Lomax AJ, et al. In-gantry or remote patient positioning? Monte Carlo simulations for proton therapy centers of different sizes. Radiother Oncol 2012;103(1):18–24.

[6] Pella A, Riboldi M, Tagaste B, Bianculli D, Desplanques M, Fontana G, et al. Commissioning and quality assurance of an integrated system for patient positioning and setup verification in particle therapy. Technol Cancer Res Treat 2014;13(4):303–14.

[7] Landry G, Hua C. Current state and future applications of radiological image guidance for particle therapy. Med Phys 2018;45:e1086–95.

[8] Bolsi A, Lomax AJ, Pedroni E, Goitein G, Hug E. Experiences at the Paul Scherrer Institute With a Remote Patient Positioning Procedure for High-Throughput Proton Radiation Therapy. Int J Radiat Oncol Biol Phys 2008;71(5):1581–90.

[9] van Loon J, Grutters J, Macbeth F. Evaluation of novel radiotherapy technologies: what evidence is needed to assess their clinical and cost effectiveness, and how should we get it? Lancet Oncol 2012;13(4):e169–77.

[10] Lievens Y, Pijls-Johannesma M. Health economic controversy and cost-effectiveness of proton therapy. Semin Radiat Oncol 2013;23(2):134–41.

[11] Mori S, Shirai T, Takei Y, Furukawa T, Inaniwa T, Matsuzaki Y, et al. Patient handling system for carbon ion beam scanning therapy. J Appl Clin Med Phys 2012;13(6):226–40.

[12] Combs SE, Jäkel O, Haberer T, Debus J. Particle therapy at the Heidelberg Ion Therapy Center (HIT) – Integrated research-driven university-hospital-based radiation oncology service in Heidelberg, Germany. Radiother Oncol 2010;95(1): 41–4.

[13] Qubala A, Schwahofer A, Jersemann S, Eskandarian S, Harrabi S, Naumann P, et al. Optimizing the Patient Positioning Workflow of Patients with Pelvis, Limb, and Chest/Spine Tumors at an Ion-Beam Gantry based on Optical Surface Guidance. Adv Radiat Oncol 2023;8(2):101105. https://doi.org/10.1016/J.ADRO.2022.101105.

[14] Stock M, Georg D, Ableitinger A, Zechner A, Utz A, Mumot M, et al. The technological basis for adaptive ion beam therapy at MedAustron: Status and outlook. Z Med Phys 2018;28(3):196–210.

[15] Fattori G, Riboldi M, Pella A, Peroni M, Cerveri P, Desplanques M, et al. Image guided particle therapy in CNAO room 2: Implementation and clinical validation. Phys Medica 2015;31(1):9–15.

[16] Rossi S. The status of CNAO. Eur Phys J Plus 2011;126(8).

[17] Orecchia R, Vitolo V, Fiore MR, Fossati P, Iannalfi A, Vischioni B, et al. Proton beam radiotherapy: Report of the first ten patients treated at the "centro Nazionale di Adroterapia Oncologica (CNAO)" for skull base and spine tumours. Radiol Medica 2014;119(4):277–82.

[18] Mirandola A, Molinelli S, Vilches Freixas G, Mairani A, Gallio E, Panizza D, et al. Dosimetric commissioning and quality assurance of scanned ion beams at the Italian National Center for Oncological Hadrontherapy. Med Phys 2015;42(9): 5287–300.

[19] Ohnesorge B, Flohr T, Schwarz K, Heiken JP, Bae KT. Efficient correction for CT image artifacts caused by objects extending outside the scan field of view. Med Phys 2000;27:39–46. https://doi.org/10.1118/1.598855.

[20] Desplanques M, Tagaste B, Fontana G, Pella A, Riboldi M, Fattori G, et al. A comparative study between the imaging system and the optical tracking system in proton therapy at {CNAO}. J Radiat Res 2013;54(suppl 1):i129–35.

[21] Fattori G, Riboldi M, Desplanques M, Tagaste B, Pella A, Orecchia R, et al. Automated fiducial localization in CT images based on surface processing and geometrical prior knowledge for radiotherapy applications. IEEE Trans Biomed Eng 2012;59(8):2191–9.

[22] Wang G. X-ray micro-CT with a displaced detector array. Med Phys 2002;29: 1634–6. https://doi.org/10.1118/1.1489043.

[23] Cho PS, Rudd AD, Johnson RH. Cone-beam CT from width-truncated projections. Comput Med Imaging Graph 1996;20(1):49–57.

[24] Belotti G, Rit S, Baroni G. Extension of the cone-beam CT field-of-view using two short scans with displaced centers of rotation. Https://DoiOrg/101117/122646384 2022;12304:81–6. https://doi.org/10.1117/12.2646384.

[25] Karius A, Szkitsak J, Strnad V, Fietkau R, Bert C. Cone-beam CT imaging with laterally enlarged field of view based on independently movable source and detector. Med Phys 2023;50(8):5135–49.

[26] Ricotti R, Pella A, Tagaste B, Elisei G, Fontana G, Bonora M, et al. Long-time clinical experience in patient setup for several particle therapy clinical indications: Management of patient positioning and evaluation of setup reproducibility and stability. Br J Radiol 2020;93. https://doi.org/10.1259/BJR.20190595/SUPPL_FILE/BJR.20190595.SUPPL-01.TIFF.

[27] Steininger P, Neuner M, Weichenberger H, Sharp GC, Winey B, Kametriser G, et al. Auto-masked 2D/3D image registration and its validation with clinical cone-beam computed tomography. Phys Med Biol 2012;57(13):4277–92.

[28] Sharp GC, Kandasamy N, Singh H, Folkert M. GPU-based streaming architectures for fast cone-beam CT image reconstruction and demons deformable registration. Phys Med Biol 2007;52(19):5771–83.

[29] Feldkamp LA, Davis LC, Kress JW. Practical cone-beam algorithm. J Opt Soc Am A 1984;1:612–9.

[30] Rit S, Oliva MV, Brousmiche S, Labarbe R, Sarrut D, Sharp GC. The Reconstruction Toolkit (RTK), an open-source cone-beam CT reconstruction toolkit based on the Insight Toolkit (ITK). J Phys Conf Ser 2014;489:12079.

[31] Fahrig R, Holdsworth DW. Three-dimensional computed tomographic reconstruction using a C-arm mounted XRII: Image-based correction of gantry motion nonidealities. Med Phys 2000;27:30–8. https://doi.org/10.1118/1.598854.

[32] Cho Y, Moseley DJ, Siewerdsen JH, Jaffray DA. Accurate technique for complete geometric calibration of cone-beam computed tomography systems. Med Phys 2005;32:968–83. https://doi.org/10.1118/1.1869652.

[33] Karius A, Karolczak M, Strnad V, Bert C. Technical evaluation of the cone-beam computed tomography imaging performance of a novel, mobile, gantry-based X-ray system for brachytherapy. J Appl Clin Med Phys 2022;23. https://doi.org/10.1002/ACM2.13501.